# Isotopic Composition of Gaseous Elemental Mercury in the Marine Boundary Layer of East China Sea

Xuewu Fu[1] , Xu Yang[2] , Qingyou Tan[1], Lili Ming[3], Tian Lin[1], Che-Jen Lin[1,4], Xiangdong Li[3] ,and Xinbin Feng[1]

[1] State Key Laboratory of Environmental Geochemistry, Institute of Geochemistry, Chinese Academy of Sciences, Guiyang, China

[2] Observatoire Midi-Pyrénées, Laboratoire Géosciences Environnement Toulouse, CNRS/IRD/Université de Toulouse, Toulouse, France

[3] Department of Civil and Environmental Engineering, The Hong Kong Polytechnic University, Kowloon, Hong Kong

[4] Center for Advances in Water and Air Quality, Lamar University, Beaumont, TX, USA

## ABSTRACT

Characterizing the speciation and isotope signatures of atmospheric mercury (Hg) downwind of mainland China is critical to understanding the outflow of Hg emission and the contributing sources. In this study, we measured the concentrations of gaseous elemental mercury (GEM), particulate bound mercury, gaseous oxidized mercury, and the GEM isotopic composition in the marine boundary layer of East China Sea from October 2013 to January 2014. Mean (±1σ) GEM, particulate bound mercury, and gaseous oxidized mercury concentrations were 2.25 ± 1.03 ng/m$^3$, 26 ± 38 pg/m$^3$, and 8 ± 10 pg/m$^3$, respectively. Most events of elevated GEM are associated with the outflow of Hg emissions in mainland China. The 24- and 48-hr integrated GEM samples showed large variations in both $\delta^{202}$Hg (—1.63‰ to 0.34‰) and $\Delta^{199}$Hg (—0.26‰ to—0.02‰). GEM $\delta^{202}$Hg and $\Delta^{199}$Hg were negatively and positively correlated to its atmospheric concentrations, respectively, suggesting a binary physical mixing of regional background GEM and Hg emissions in mainland China. Using a binary mixing model, highly negative $\delta^{202}$Hg (—1.79 ± 0.24‰, 1σ) and near-zero $\Delta^{199}$Hg (0.02 ± 0.04‰, 1σ) signatures for China GEM emissions are predicted. Such isotopic signatures are significantly different from those found in North America and Europe and the background global/regional atmospheric GEM pool. It is likely that emissions from industrial and residential coal combustion (lacking conventional air pollutant control devices), cement and mercury production, biomass burning, and soil emissions contributed significantly to the estimated isotope signatures of GEM emissions in China.


## INTRODUCTION

Mercury (Hg) is a toxic pollutant to humans and wildlife. The levels and isotopic compositions

of Hg in the Earth's surface reservoirs largely depend on the transformation and transport of Hg in the atmosphere (Blum et al., 2014; Lamborg et al., 2014). Both anthropogenic and natural sources contribute to Hg release into the atmosphere. Anthropogenic sources emit 1,900–2,300 tons of Hg annually (Pacyna et al., 2010; Pirrone et al., 2010), representing approximately one third of global total Hg emissions, whereas the remaining frac- tion comes from natural sources and reemission of deposited Hg (Selin et al., 2007). Atmospheric Hg occurs predominantly in the form of gaseous elemental mercury (GEM), while other forms including gaseous oxidized mercury (GOM) and particulate bound mercury (PBM) generally account for <10% of total Hg in the atmosphere (Gustin et al., 2015). Because of its mild reactivity, high volatility, and low water solubility, GEM is fairly stable with an atmospheric lifetime of several months to a year and can spread globally before deposited to the Earth's surfaces (Lindberg et al., 2007). In contrast, GOM and PBM have much higher dry deposition velocity and water solubility and can be readily removed from the atmosphere (Wright et al., 2016; Zhang et al., 2016).

Hg has seven stable isotopes with atomic mass ranging from 196 to 204 (Bergquist & Blum, 2007). Since the development of multicollector inductively coupled plasma mass spectrometry (MC-ICPMS) method and improvements of sample collection and processing, important advances have been achieved in the measure- ment of Hg isotopic compositions in geogenic and environmental samples (Blum et al., 2014). The reported mass-dependent Hg isotope fractionation (MDF, $\delta^{202}$Hg signature) and mass-independent fractionation (MIF, $\Delta^{199}$Hg, $\Delta^{201}$Hg signatures) of odd Hg isotopes varied significantly in a range exceeding 10‰ (Blum et al., 2014; Sonke & Blum, 2013). The observed fractionation and variability have been attributed to environmental processes including reduction/oxidation, methylation/demethylation, adsorption/desorption, or evaporation (Bergquist & Blum, 2007; Estrade et al., 2009; Kritee et al., 2008; Rodriguez-Gonzalez et al., 2009;

Wiederhold et al., 2009; Zheng et al., 2007; Zheng & Hintelmann, 2009). The unusual MIF of even Hg isotopes ($\Delta^{200}$Hg, $\Delta^{204}$Hg signatures) has been also observed in precipitation and atmospheric GEM, PBM, and GOM (Chen et al., 2012; Demers et al., 2013; Gratz et al., 2010; Rolison et al., 2013). Although the environmental processes driving the MDF and MIF of Hg isotopes need to be further investigated, the isotopic signature serves as an important signal for tracing the sources, transformation, and cycling of Hg in the environment (Blum et al., 2014).

Recently, several studies have reported isotopic compositions of total gaseous mercury (TGM = GEM + GOM) in the planetary boundary layer (PBL) and in the free troposphere in North America and Europe (Demers et al., 2013, 2015; Enrico et al., 2016; Fu, Marusczak, Wang, et al., 2016; Gratz et al., 2010; Obrist et al., 2017; Sherman et al., 2010). These studies found that $\delta^{202}$Hg of TGM from anthropogenic sources is lower than the value observed in the background atmospheric Hg pool, which is characterized by moderately positive $\delta^{202}$Hg values (Demers et al., 2015; Fu, Marusczak, Wang, et al., 2016; Gratz et al., 2010). Processes including foliar uptake and oxidation of atmospheric GEM have been suggested to be responsible for the positive $\delta^{202}$Hg of TGM in the global Hg background (Demers et al., 2013; Fu, Marusczak, Wang, et al., 2016). China is the single largest source country of atmospheric Hg in the world (Pacyna et al., 2010; Pirrone et al., 2010), and therefore, its emissions play an important role in the global cycling of atmospheric Hg. As a newly industria- lizing country, proportion of anthropogenic Hg emissions from various source sectors in China are different from those in Europe and North America. For example, emission from coal-fired power plants (CFPPs) is the dominant anthropogenic Hg source in Europe and North America, accounting for 55–70% of the total anthropogenic Hg emissions in these regions (Muntean et al., 2014), and these values are much higher than that (18.8%) in China (Zhang et al., 2015). In China, anthropogenic Hg emissions are mainly

derived from industrial and residential coal combustion, nonferrous metal smelting, and cement production, accounting for 63.3% of the total anthropogenic Hg emissions (Zhang et al., 2015). Isotopic signatures of Hg emitted anthropogenic sources could be influenced by the isotopic signatures of Hg in different source materials and air pollution control devices (APCDs; Sun, Heimburger, et al., 2013; Sun et al., 2016). Application rates of APCDs in industrial and residential coal combustion are much lower than CFPPs (Wu et al., 2016) and would therefore not induce significant positive shifts of $\delta^{202}$Hg of emitted GEM relative to feed source materials as that of CFPPs (Sun et al., 2016). Isotopic compositions of GEM emitted from zinc smelting and cement production were esti- mated to have much more negative $\delta^{202}$Hg values than that emitted from CFPPs (Sun et al., 2016; Tang et al., 2017). As a consequence, isotopic signatures of Hg emitted from Chinese anthropogenic sources would differ from those in North America and Europe. Hence, there is a need to study the isotopic compositions of atmospheric Hg in China for characterizing the isotopic compositions of Hg emissions in China and back- ground regional atmospheric Hg pool, which in turn helps to understand the impact of Chinese emission on regional/global atmospheric Hg budget.

Dynamics of atmospheric Hg in the marine boundary layer (MBL) is of interest because of the large fraction of GEM emitted from the ocean and the enhanced atmospheric GEM oxidation (Laurier et al., 2003; Mao et al., 2016; Strode et al., 2007; Wang et al., 2014). A pervious TGM isotope study in the Grand Bay, Mississippi, USA, showed highly negative $\delta^{202}$Hg (<2‰) in oceanic air masses, reflecting photoreduction, and evasion of Hg from the ocean (Rolison et al., 2013). Recent studies in the coastal Pensacola, Florida, USA, and the Pic du Midi Observatory, France, however, suggest that oceanic air mass is characterized by moderate positive TGM $\delta^{202}$Hg (means of 0.77‰ and 0.43‰, respectively; Demers et al., 2015; Fu, Marusczak,

Wang, et al., 2016), which were likely a result of atmospheric oxidation that increases GEM $\delta^{202}$Hg in the heavier isotopes (Fu, Marusczak, Wang, et al., 2016).

In the present study, concentrations and isotopic composition of atmospheric GEM were measured at Huaniao Island (HNI) in the MBL of East China Sea (ECS). To the best of our knowledge, this is the first study to directly measure GEM isotopic composition in the MBL. HNI regularly receives Hg-polluted air masses originated from the PBL of mainland China and clean air masses from the West Pacific Ocean (Figure S1). The observations provide an insight into the isotopic signatures of Hg sources in mainland China and the back- ground atmospheric Hg pool in East Asia as well as the sources of atmospheric Hg in the MBL of ECS.

## MATERIALS AND METHODS

### Site Description

HNI (30.86°N, 122.67°E) is a small island (3.2 $km^2$) located in the ECS and approximately 66 km east of shore of Shanghai (Figure S1). The sampling site was located on the north edge of HNI and approximately 50 m from the ocean. There were no industrial activities and fossil fuel consumption at HNI. The population in HNI is ~800 and mostly concentrated in the southwest of HNI, which plays a minor role in the observations under the dominant northwestern monsoonal wind during the study period.

### Atmospheric Hg Speciation Measurements

Atmospheric GEM, PBM, and GOM at 5 m above ground level were continuously measured using the Tekran® 2537/1130/1135 system (Tekran Inc., Canada) from 22 October 2013 to 6 January

2014 (Malcolm et al., 2003). Atmospheric GOM and PBM were collected onto KCl-coated annular denuder and quartz fiber filter in sequence at 1-hr intervals at a volumetric flow rate of 10 L/min (LPM). During the collection of GOM and PBM, GEM was trapped by dual gold cartridges at 5-min interval at a mass flow rate of 1.0 LPM and subsequently thermally decomposed and detected by the cold vapor atomic fluorescence spectroscopy (CVAFS). Once collected, GOM and PBM are thermally decomposed from each unit and detected by CVAFS as $Hg^0$. KCl-coated denuder, Teflon coated glass inlet, and impactor plate were replaced every 10 days, and quartz filters were replaced every 20 days. Denuders and quartz filters were prepared and cleaned before field sampling following the methods in Tekran technical notes. The Tekran® 2537 analyzer was routinely calibrated using its internal permeation source at a 47-hr interval.

**Backward Trajectory and Potential Source Identification at HNI**

The potential source regions of elevated atmospheric GEM (>1.5 ng/m$^3$) observed at HNI are identified using a Potential Source Contribution Function (PSCF) approach (Fu, Marusczak, Heimburger, et al., 2016), based on the every 2-hr calculations of seven-day backward trajectories ending at HNI using the TrajStat Geographical Information System based software (Wang et al., 2009). The criterion of the elevated GEM (>1.5 ng/m$^3$) is when the concentration is greater than the background GEM concentrations in the Northern Hemisphere (Sprovieri et al., 2016). We also identified the potential source regions of low atmospheric GEM (<1.5 ng/m$^3$) at HNI using the PSCF approach. To differentiate from the potential source regions associated with elevated atmospheric GEM (indicated by the PSCF values), the potential source regions of low atmospheric GEM are indicated by Potential Background Contribution Function (PBCF) values. Fractional atmospheric air masses residence time (ARTs, i.e., the percent of time an air mass

spent over different regions) over mainland China, other continents in Asia (including Russia), and oceans (mostly of the ECS, Yellow Sea, and West Pacific Ocean) were estimated from seven-day backward trajectories. The three-dimensional locations of air masses predicted by backward trajectory have an uncertainty of up to 40% for seven-day trajectories (Engstrom & Magnusson, 2009). However, given the large number of trajectory endpoints utilized in PSCF and PBCF modeling, the uncertainty of the locations of identified source region is substantially reduced. Besides, the "trailing effect," selection of concentration threshold, transformation, and deposition of atmospheric Hg during transport can affect the PSCF and PBCF receptor model (Cheng et al., 2015), which were not evaluated in the present study. Therefore, the identified source regions of elevated and low atmospheric GEM should be regarded as potential source contributors only.

**GEM Collections and Processing for Isotope Analysis**

TGM at HNI was collected on chlorine-impregnated activated carbon (CLC, 1.0 g) traps at volumetric flow rates of 10–12 LPM. Detailed information regarding the preparation of CLC can be found in Fu et al.(2014). Atmospheric TGM consists of GEM and GOM. Under the sampling conditions (24 and 48 hr) in this study, GOM generally made up a small portion of TGM (on average 0.35% of TGM and never exceeds 1.3%). Recent studies suggested that GOM concentrations measured by KCl-coated denuders can be under-estimated by a factor of 2 to 3 (Gustin et al., 2015). The average fraction of GOM in TGM could therefore increase up 1.0% and temporarily up to 3.9%. Therefore, the minor fraction of GOM in TGM at HNI is unlikelyto bias the measured TGM isotopic composition, which is equivalent to the GEM isotopic compositions. Blanks of the CLC traps were determined with values <0.4 ng ($n$ = 8), negligible compared to the amount of GEM collected during field sampling (10–55.3 ng Hg per sample).

GEM collection recoveries of the CLC traps at flow rates of 10–12 LPM were determined by measuring the breakthrough of GEM during a sampling period of 24 hr (i.e., we used a CLC trap that consists of two sections within the same trap to estimate the GEM sampling efficiency. The second section (downstream of the first section which contains 1.0 g of CLC) containing of 0.2 g of CLC was used to measure breakthrough concentrations. The collection efficiency can be defined as GEM concentrations measured by the first section relative to the sum of first and second sections. The collection recoveries of the CLC traps were in the range of 97.4–99.8% (mean [$\pm 1\sigma$] = 98.4 ± 1.0% [$n = 6$]). Atmospheric particles were removed using a 47-mm diameter Teflon filter (pore size 0.2 μm) installed at the inlet of CLC traps. CLC traps were kept warm (50–70 °C) during sampling to avoid water condensation. Sampling of GEM isotopes was conducted from 21 October to 25 November 2014 and from 13 to 23 December 2014 with sampling durations of 24 and 48 hr, respectively. After the field sampling, CLC traps were sealed carefully and kept in a clean environment until preconcentration into trap solutions for Hg isotope analysis.

GEM collected on CLC traps was preconcentrated into 5–10 ml of 40% mixed acid solution (v/v, $2HNO_3$/ 1HCl) using a double-stage combustion protocol described before for Hg isotope analysis (Biswas et al., 2008; Sun, Enrico, et al., 2013). Briefly, GEM in CLC traps was thermally released through combustion using a Hg-free oxygen flow (25 ml/min), and then the combustion products were further decomposed in a hot quartz tube (1000 °C). The combustion released all the Hg in the form of $Hg^0$, which was subsequently sparged into mixed acid solution. After the completion of the combustion, the trapping bottles and impin- gers were rinsed 3 times with Milli-Q water. The rinsed water was added to trapping solutions to yield an acid concentration of ~20% for Hg isotope analysis. The final trapping solutions were kept in a refrigerator at 2–4 °C until the isotope analysis. Full procedural blanks of the combustion system

and CLC traps were investigated by combustion of 1.0 g of CLC and showed a mean (±1σ) of 0.034 ± 0.007 ng/ml ($n$ = 4), which accounted for a mean (±1σ) of 2.2 ± 0.8% of Hg concentrations in filed sample trapping solutions. The recov- eries of preconcentration of CLC traps were tested by combusting standard reference material BCR 482 (lichen, 480 ng/g) using the same combustion protocol of CLC traps. Mean (±1σ) recoveries of the combus- tion was 94.3 ± 3.6% ($n$ = 4).

**Mercury Isotope Analysis**

Hg isotope ratios were measured using cold vapor MC-ICPMS (Thermo-Finnigan Neptune) at the State Key Laboratory of Ore Deposit Geochemistry, CAS, Guiyang, China, following the method described in a previous study (Yin et al., 2010). Instrumental mass bias of MC-ICPMS was corrected by standard- sample-standard bracketing using NIST 3133 Hg at matching concentrations. Hg isotopic composition is reported in delta notation (δ) in per mil referenced to the bracketed NIST 3133 Hg standard (Blum & Bergquist, 2007):

$$\delta^{xxx}\mathrm{Hg} = \left(\frac{\left(^{xxx}\mathrm{Hg}/^{198}\mathrm{Hg}\right)_{\mathrm{sample}}}{\left(^{xxx}\mathrm{Hg}/^{198}\mathrm{Hg}\right)_{\mathrm{SRM3133}}} - 1\right) \times 1000‰ \quad (1)$$

MIF values are expressed by "capital delta (Δ)" notation (‰), which is the difference between the measured values of $\delta^{199}$Hg, $\delta^{200}$Hg, $\delta^{201}$Hg, and those predicted from $\delta^{202}$Hg using the kinetic MDF law (Blum & Bergquist, 2007):

$$\Delta^{199}\mathrm{Hg}\ (‰) = \delta^{199}\mathrm{Hg} - \left(0.252 \times \delta^{202}\mathrm{Hg}\right) \quad (2)$$

$$\Delta^{200}\mathrm{Hg}\ (‰) = \delta^{200}\mathrm{Hg} - \left(0.502 \times \delta^{202}\mathrm{Hg}\right) \quad (3)$$

$$\Delta^{201}\mathrm{Hg}\ (‰) = \delta^{201}\mathrm{Hg} - \left(0.752 \times \delta^{202}\mathrm{Hg}\right) \quad (4)$$

The analytical uncertainty of isotopic analysis was obtained by repeated analysis of the UM-

222 Almaden stan- dard over different analysis. The overall mean (±2σ) values of $\delta^{202}$Hg, $\Delta^{199}$Hg,
223 $\Delta^{200}$Hg, and $\Delta^{201}$Hg for all the UM-Almaden standards were 0.54 ± 0.08‰, 0.01 ± 0.06‰,
224 0.01 ± 0.06‰, and 0.01 ± 0.08‰ ($n$ = 15), respectively, in excellent agreement with previously
225 reported values (Blum & Bergquist, 2007). Mean (±2σ) values of $\delta^{202}$Hg, $\Delta^{199}$Hg, $\Delta^{200}$Hg, and
226 $\Delta^{201}$Hg for the standard reference material BCR 482 were 1.65 ± 0.17‰, 0.61 ± 0.06‰, 0.07 ±
227 0.03‰, and 0.64 ± 0.10‰ ($n$ = 4), which were comparable with lit- erature data (Estrade et al.,
228 2010). The analytical uncertainty of isotopic composition of GEM samples in this study is
229 represented as the larger 2σ values from either the analytical replicates or the measurements of UM-
230 Almaden standards.

231

232 **RESULTS AND DISCUSSION**

233 **Hg Speciation and Sources**

234 Mean (±1σ) atmospheric GEM, PBM, and GOM concentrations at HNI during the study
235 period were 2.25 ± 1.03 ng/m$^3$, 26 ± 38 pg/m$^3$, and 8 ± 10 pg/m$^3$, respectively. Atmospheric Hg
236 varied significantly with the maximum GEM (5-min mean), PBM (hourly mean), and GOM
237 (hourly mean) concentrations of 13.9 ng/m$^3$, 422 pg/m$^3$, and 97 pg/m$^3$, respectively (Figure S2).
238 The mean GEM, PBM, and GOM levels at HNI were consistent with observations in remote areas
239 of China (Fu et al., 2015) but relatively higher than those observed in MBL in the North Pacific
240 Ocean, Mediterranean Sea, East Pacific Ocean, Subtropical Atlantic Ocean, and South Indian
241 Ocean (GEM = 0.85 to 2.04 ng/m$^3$, PBM = 1 to 3 pg/m$^3$, and GOM = 2 to 8 pg/m$^3$; Chand et al.,
242 2008; Laurier & Mason, 2007; Mao et al., 2016; Slemr et al., 2015; Sprovieri et al., 2003; Wang
243 et al., 2014).

244 Our measurements reveal that outflow of Hg from mainland China was the major source of

atmospheric GEM at HNI (Figure 1). The major source regions of elevated atmospheric GEM at HNI were dominantly from the PBL over eastern and central China, including Shanghai metropolitan area, Jiangsu, Zhejiang, Anhui, Shandong, Henan, Hubei, and Jiangxi provinces (Figures 1 and S3). The total anthropogenic Hg emissions in these regions were estimated to be 208 tons in 2010, accounting for 39.3% of the total anthropogenic Hg emissions in China (Zhang et al., 2015). On the other hand, low atmospheric GEM at HNI was mostly associated with air mass from the open seas of ECS, the Yellow Sea, and the free troposphere over Northeast Asia (Figures 1 and S3).

**GEM Isotopic Compositions**

Isotopic compositions of atmospheric GEM at HNI ($n$ = 34) varied from 1.63‰ to 0.34‰ (mean [±1σ] = 0.21 ± 0.39‰) for $\delta^{202}$Hg, 0.26‰ to 0.02‰ (mean [±1σ] = 0.16 ± 0.06‰) for $\Delta^{199}$Hg, 0.11‰ to 0.03‰ (mean [±1σ] = 0.06 ± 0.03‰) for $\Delta$ Hg, and 0.32‰ to 0.08‰ (mean [±1σ] = 0.18 ± 0.08‰) for $\Delta^{201}$Hg (Figure 2 and Table S1). A comparison of the isotopic compositions of atmospheric TGM/GEM between this and previous studies is shown in Table S2 in the supporting information (Demers et al., 2013, 2015; Enrico et al., 2016; Fu, Marusczak, Wang, et al., 2016; Fu, Zhu, et al., 2016; Gratz et al., 2010; Obrist et al., 2017; Rolison et al., 2013; Sherman et al., 2010; Xu et al., 2017; Yu et al., 2016). The $\delta^{202}$Hg values of GEM at HNI were much lower than those measured in the free troposphere of Pic du Midi Observatory (mean [±1σ] = 0.17 ± 0.14‰) and forested Pinet peat bog (mean [±1σ] = 1.19 ± 0.13‰) in France and those in the Great Lakes region (mean [±1σ] = 0.21 ± 0.30‰), Wisconsin forest (mean [±1σ] = 0.75 ± 0.24‰), coastal region of Pensacola, Florida (mean [±1σ] = 0.84 ± 0.25‰), and Alaska (mean [±1σ] = 0.67 ± 0.09‰) in the United States (Demers et al., 2013, 2015; Enrico et

al., 2016; Fu, Marusczak, Wang, et al., 2016; Gratz et al., 2010; Obrist et al., 2017) but higher than or comparable to those measured in urban Beijing (mean [±1σ] = 0.73 ± 0.57‰), Guiyang (mean [±1σ] = 0.56 ± 0.21‰), and Xi'an (mean [±1σ] = 0.08 ± 0.41‰), China (Xu et al., 2017; Yu et al., 2016). The $\Delta^{199}$Hg values of GEM at HNI were com- parable to the observations at remote sites in the United States (e.g., the Great Lake region, mean [±1σ] = 0.12 ± 0.06‰; Wisconsin forest, mean [±1σ] = 0.19 ± 0.03‰; coastal region of Pensacola, Florida, mean [±1σ] = 0.23 ± 0.05‰; and Alaska, mean [±1σ] = 0.25 ± 0.04‰) and France (e.g., the Pic du Midi Observatory, mean [±1σ] = 0.21 ± 0.03‰, and forested Pinet peat bog, mean [±1σ] = 0.17 ± 0.07‰; Demers et al., 2013, 2015; Enrico et al., 2016; Fu, Marusczak, Wang, et al., 2016; Gratz et al., 2010; Obrist et al., 2017) but slightly lower than those measured in urban Beijing (mean [±1σ] = 0.03 ± 0.07‰), Guiyang (mean [±1σ] = 0.04 ± 0.05‰), and Xi'an (mean [±1σ] = 0 ± 0.04‰), China (Xu et al., 2017; Yu et al., 2016).

Global observations indicate significant variations in $\delta^{202}$Hg (2.03 to 1.43‰) and $\Delta^{199}$Hg (0.31 to 0.15‰). Regional mean GEM $\delta^{202}$Hg rank in a descending order at U.S. remote sites, European remote sites, MBL of ECS, and then Chinese urban sites, whereas global spatial variations of GEM $\Delta^{199}$Hg are in a reverse order with more negative $\Delta^{199}$Hg observed in the United States and at remote European sites, and $\Delta^{199}$Hg near zero in Chinese urban areas (Figure 2). These variations can be attributed to a number of reasons including the dif- ferent proportions of background global atmospheric Hg pool and regional emissions contributing to the atmospheric GEM budget, in situ atmospheric Hg transformations, and the specific isotopic signatures of Hg emissions from different regions. Due to the large domestic anthropogenic Hg emissions, modeling stu- dies estimated that local anthropogenic sources contributed at least 30% to the surface GEM concentrations in mainland China, and this value is higher than that in the nearshore

zone and open seas of ECS (10–30%), Europe (11.3%), and North America (5.5%; Chen et al., 2015, 2014). GEM originated from global anthropogenic sources has moderately negative $\delta^{202}$Hg (mean = 0.59‰) and $\Delta^{199}$Hg close to zero (mean = 0.02‰; Sun et al., 2016), which are significantly lower and higher than the $\delta^{202}$Hg (mean [±1σ] = 0.84 ± 0.22‰) and $\Delta^{199}$Hg (mean [±1σ] = 0.21 ± 0.04‰) of atmospheric GEM observed in remote areas not affected by direct anthropogenic emissions (e.g., Wisconsin forest, coastal region of Pensacola impacted by oceanic and free tropospheric air, and Alaska in the United States and forested Pinet peat bog in France), respectively (Demers et al., 2013, 2015; Enrico et al., 2016; Obrist et al., 2017). Therefore, the large proportions of local anthropogenic emissions in atmospheric GEM budget in mainland China and MBL of ECS drive the GEM isotopic compositions toward lower $\delta^{202}$Hg and higher $\Delta^{199}$Hg values. GEM isotopic compositions could also be modified by natural environmental processes. Atmospheric GEM in forests worldwide generally had positive $\delta^{202}$Hg values mainly due to the preferential uptake of lighter isotopes by foliage (Demers et al., 2013; Enrico et al., 2016; Fu, Zhu, et al., 2016). Oceanic emission and oxidation of atmospheric GEM are the two important processes influencing the atmospheric GEM dynamics in MBL. Modeled contribution of oceanic emission to atmospheric GEM concentrations in the MBL of ECS is ranging from 20 to 40% (Soerensen et al., 2010). The isotopic composition of GEM emitted from ocean is poorly constrained. However, previous studies analyzed the air masses from ocean and suggested that GEM in MBL was characterized by moderately positive $\delta^{202}$Hg values (Demers et al., 2015; Fu, Marusczak, Wang, et al., 2016). Hence, mixing of clean oceanic air masses would probably result in higher $\delta^{202}Hg_{GEM}$ at HNI compared to Chinese urban areas. It should also be noted that two GEM samples at HNI were observed with $\delta^{202}$Hg values (1.09‰ and 1.63‰ scientifically lower than the average δ HG (0.59‰) of global anthropogenic emission

sources. These samples were mainly impacted by outflow of Hg from mainland China and indicated that Hg emissions from mainland China may have much lower $\delta^{202}$Hg values relative to the mean of global anthropogenic emission sources, which is further discussed in the following sections.

**Relationship Between Concentrations of Atmospheric Hg and GEM Isotopic Composition**

The $\delta^{202}$Hg of GEM was negatively correlated with GEM concentrations, while the $\Delta^{199}Hg_{GEM}$ showed positive correlation with GEM concentra- tions at HNI during the study period (Figure 3). The correlations suggest a binary mixing of end-member sources, with one end-member characterized as elevated GEM concentra- tions, highly negative GEM $\delta^{202}$Hg, and near-zero GEM $\Delta^{199}$Hg values and the other end-member character- ized as low GEM concentrations, moderately positive GEM $\delta^{202}$Hg, and negative GEM $\Delta^{199}$Hg values. A recent GEM isotope study at the Pic du Midi Observatory, France, observed higher GEM $\delta^{202}$Hg for free tropospheric Atlantic Ocean air masses with elevated GOM concentrations but not for the Atlantic MBL air masses (Fu, Marusczak, Wang, et al., 2016). In this study, no significant relationship was found between atmospheric GOM concentrations and $\Delta^{199}Hg_{GEM}$ or $\delta^{202}Hg_{GEM}$ (Figure S4; *p* values for both >0.05). This suggests that mixing of sources and/or air masses rather than atmospheric GEM oxidation was the main cause for the variation of GEM isotopic compositions in the MBL of ECS.

During the campaign at HNI, air masses mainly originated from mainland China (mean fractional ARTs = 25%), other Asian regions (mean fractional ARTs = 41%), and oceans (e.g., ECS, Yellow Sea, and West Pacific Ocean, mean fractional ARTs = 34%). Identified potential source regions suggested that elevated GEM concentrations at HNI were mostly associated with the outflow

337 from mainland China (Figure 1). In addition, the GEM $\delta^{202}$Hg values were significantly
338 negatively correlated with fractional Chinese ARTs ($r^2$ = 0.31, $p$ < 0.01) and no significant
339 relationship existed between GEM $\Delta^{199}$Hg values and fractional Chinese ARTs ($r^2$ = 0.05, $p$ =
340 0.21; Figure S5). Due to the impacts of domestic emissions, previous studies in urban China
341 observed highly elevated GEM concentrations (mean [±1σ] = 9.20 ± 7.56 ng/m$^3$), negative
342 GEM $\delta^{202}$Hg (mean [±1σ] = 0.40 ± 0.51‰), and near-zero GEM $\Delta^{199}$Hg (mean [±1σ] = 0.00 ±
343 0.06‰; Fu et al., 2015; Xu et al., 2017; Yu et al., 2016). These findings suggest that Chinese
344 emissions represented an end-member source at HNI (hereafter, referred to as Chinese sources,
345 characterized by elevated GEM concentration, highly negative GEM $\delta^{202}$Hg, and near-zero GEM
346 $\Delta^{199}$Hg). In contrast, low GEM concentrations at HNI were mainly associated with air masses
347 from open seas of ECS and Yellow Sea and the Asian free troposphere (Figure 1). This is
348 consistent with previous modeling results that atmospheric GEM concentrations in these regions
349 ranged from 1.2 to 1.6 ng/m$^3$ (Lin et al., 2010; Pan et al., 2010). Based on the correlations between
350 GEM concentrations and GEM isotopic compositions observed in this study, it is likely that open
351 seas and the Asian free troposphere represented the other end-member source at HNI (hereafter,
352 referred to as regional background, characterized by low GEM concentration, moderately
353 positive $\delta^{202}Hg_{GEM}$, and negative $\Delta^{199}Hg_{GEM}$). These regions receive little (e.g., <20%) influence
354 from anthropogenic emissions and therefore represent regional background atmospheric pool
355 (Pan et al., 2010). Clear difference in GEM isotope MDF ($\delta^{202}$Hg) signatures between emission
356 sources and regional background atmospheric pool has been observed in Europe and North
357 America (Demers et al., 2015; Fu, Marusczak, Wang, et al., 2016; Gratz et al., 2010). To our
358 knowledge, this is the first study identifying that distinguishable MDF ($\delta^{202}$Hg) and MIF ($\Delta^{199}$Hg)
359 signatures of GEM exist between emission sources in mainland China and the background

360 atmospheric pool in East Asia.

361 Similar relationships between GEM concentrations and GEM $\delta^{202}$Hg were also observed in North
362 America and Europe (Figure 3). Observations in North America and Europe generally showed
363 lower GEM concentrations (0.84 to 1.99 ng/m$^3$), positive GEM $\delta^{202}$Hg, and moderately negative
364 $\Delta^{199}$Hg (Demers et al., 2013, 2015; Enrico et al., 2016; Fu, Marusczak, Wang, et al., 2016; Obrist
365 et al., 2017), while observations in this study showed higher GEM concentrations (1.53 to 3.72
366 ng/m$^3$), lower GEM $\delta^{202}$Hg, and higher $\Delta^{199}$Hg values. The correlation slopes of
367 $\delta^{202}$Hg/GEM$_{conc.}$ ( 0.61 ± 0.08‰/(ng/m$^3$)) and $\Delta^{199}$Hg/GEM$_{conc.}$ (0.07 ± 0.02‰/ ng/m$^3$) in ECS
368 differ from those in Europe ($\delta^{202}$Hg/GEM$_{conc.}$ correlation slope = 1.42 ± 0.12‰/ng/m$^3$; and no
369 significant relationship existed between GEM $\Delta^{199}$Hg and concentrations) and North America (no
370 significant relationship existed between GEM $\delta^{202}$Hg, $\Delta^{199}$Hg, and GEM concentrations; Figure
371 3). It should be noted that 70% of the GEM samples in North America and Europe had
372 concentrations lower than the back- ground values (1.53 ng/m$^3$) in the Northern Hemisphere
373 (Sprovieri et al., 2016), whereas all the GEM samples at HNI had concentrations higher than the
374 background in the North Hemisphere (Figure 3). The sampling sites in North America and Europe
375 were mostly located in the vegetation-covered regions (e.g., forest and tundra) and/or free
376 troposphere. In these regions, atmospheric transformations including foliar uptake and
377 atmospheric oxidation could deplete GEM concentration quickly (Fu, Zhu, et al., 2016;
378 Swartzendruber et al., 2006), and consequently resulted in GEM concentrations lower than the
379 background in the North Hemisphere. At the same time, foliar uptake and atmospheric oxidation
380 of GEM could shift the GEM isotopic compositions toward higher $\delta^{202}$Hg values (Demers et al.,
381 2013; Enrico et al., 2016; Fu, Marusczak, Wang, et al., 2016). Therefore, atmospheric
382 transformations should play a more important role in regulating the correlation slopes of

383 $\delta^{202}Hg/GEM_{conc.}$ in Europe and North America than mixing of sources. This is different from
384 HNI where mixing of sources played a more important role.

385

386 **Probing Isotopic Composition of GEM Emissions in China and Regional Background**
387 **Atmospheric GEM Pool**

388 The isotopic compositions of GEM emissions in mainland China and regional background
389 atmospheric GEM pool (e.g., the open seas and free troposphere in East Asia) end-members are
390 estimated using the linearized $\delta^{202}Hg$ versus $1/GEM_{conc.}$ and $\Delta^{199}Hg$ versus $1/GEM_{conc.}$ physical
391 mixing diagrams (Figure 4; Xu et al., 2017). Extrapolating $1/GEM_{conc.}$ to 0 (i.e., the air mass
392 contains a negligible fraction of background atmospheric GEM) yields a $\delta^{202}Hg$ value of —
393 1.79 ± 0.24‰ (1σ) and a $\Delta^{199}Hg$ value of 0.02 ± 0.04‰ (1σ) for the GEM emissions in
394 mainland China. The $\delta^{202}Hg$ of GEM emissions in mainland China was more negative than the
395 estimated mean value (— 0.59‰) of global anthropogenic emissions and that (— 0.44‰)
396 estimated for local anthropogenic GEM emissions in urban Xi'an in northwestern China (Sun et
397 al., 2016; Xu et al., 2017). The $\Delta^{199}Hg$ of GEM emissions in mainland China was comparable to
398 the estimated mean value (—0.02‰) of glo- bal anthropogenic emissions (Sun et al., 2016). The
399 difference in estimated $\delta^{202}Hg$ signatures between this and previous studies could be partly
400 attributed to the regional variations in proportion of Hg emissions from various emission sectors.
401 Sun et al. (2016) compiled Hg isotopic compositions of global source materials and suggested a
402 large difference in $\delta^{202}Hg$ and a small difference in $\Delta^{199}Hg$ among various emission sectors. For
403 example, due to the MDF of Hg isotopes during coal combustion in CFPPs, $\delta^{202}Hg$ value of GEM
404 emitted from CFPPs (0.54 ± 0.25‰, 1σ) was much higher than those of other emission
405 sectors such as zinc smelting (—0.76 ± 1.25‰, 1σ) and cement production (—1.64 ± 0.61‰,

406 1σ; Sun et al., 2016; Tang et al., 2017). The pro- portions of CFPPs Hg emissions in total
407 anthropogenic Hg emissions in the world (29.1%) and urban Xi'an, northwestern China (72%),
408 were much higher than the overall mean (18.8%) in China (Muntean et al., 2014; Xu et al.,
409 2017; Zhang et al., 2015), which probably increased $\delta^{202}$Hg of anthropogenic emissions in the
410 heavier isotopes. It should be noted that the estimated isotopic compositions of GEM emissions
411 in main- land China could be a result of a mixing of various sources (anthropogenic and natural
412 sources) and atmo- spheric transformation-induced fractionation of Hg isotopes in the plume
413 of Chinese outflow. In the following, we will therefore consider these factors to interpret the
414 estimated $\delta^{202}$Hg and $\Delta^{199}$Hg signatures of anthropogenic emissions in China.

415 GEM in the atmosphere can be derived from anthropogenic and natural sources. A comparison
416 of $\delta^{202}$Hg and $\Delta^{199}$Hg in major source materials between China and the rest of the world is shown
417 in Figure S6 and Table S3 in the supporting information (Biswas et al., 2008; Demers et al.,
418 2013; Lefticariu et al., 2011; Smith et al., 2008; Sonke et al., 2010; Sun et al., 2014, 2016;
419 Thibodeau et al., 2016; Yin et al., 2014, 2016, 2013; Yu et al., 2016; Zheng et al., 2016).
420 Mean (±1σ) $\Delta^{199}$Hg in feed coal, zinc ores, limestone, Hg ores, and biomass in China are —
421 0.03 ± 0.16‰, 0.02 ± 0.06‰, 0.01 ± 0.07‰, —0.01 ± 0.02‰, and — 0.19 ± 0.10‰,
422 respectively, significantly higher than those (—0.16 ± 0.18‰, 0.04 ± 0.06‰, —
423 0.03 ± 0.08‰, —0.04 ± 0.07‰, and —0.28 ± 0.09‰, respectively) in the rest of the world
424 (paired $t$ test, $p < 0.05$, $T = 3.7$, $n = 5$). Assuming that isotopic signatures of GEM emissions
425 from major anthropogenic sources resemble the MIF signatures of source materials (Sun,
426 Heimburger, et al., 2013; Sun et al., 2014,
427 2016; Tang et al., 2017), $\Delta^{199}$Hg of atmospheric GEM in mainland China, influenced by the
428 regional anthro- pogenic sources, should be higher than the GEM $\Delta^{199}$Hg in other regions

429 worldwide, as shown in Figure 2. Coal combustion in CFPPs and nonferrous metal smelting are
430 the two important sources of atmospheric GEM in China and other regions worldwide (Pirrone
431 et al., 2010; Zhang et al., 2015). The mean (±1σ) $\delta^{202}$Hg values of Chinese coal and zinc ores
432 are —1.07 ± 0.71‰ and —0.47 ± 0.47‰, respectively, less negative than those (mean
433 $[\pm1\sigma]_{\text{feed coal}}$ = —1.42 ± 9‰, mean $[\pm1\sigma]_{\text{zinc ores}}$ = —0.76 ± 0.62‰) found in the rest of the
434 world (Biswas et al., 2008; Lefticariu et al., 2011; Sonke et al., 2010; Sun et al., 2014; Yin
435 et al., 2014, 2016). Assuming that the MDF of Hg isotopes during coal combustion in CFPPs
436 (sufficiently equipped with APCDs) is more or less similar across the world; and that GEM
437 emission from zinc smelting resembles the Hg isotope composition of zinc ore (Sun et al.,
438 2016), GEM emission from CFPPs and zinc smelting in China would therefore have
439 relatively higher $\delta^{202}$Hg relative to other regions worldwide. Our study suggests an opposite
440 pattern with lower GEM $\delta^{202}$Hg of GEM emissions in China (Figure 4).

441 This discrepancy is possibly caused by other anthropogenic Hg sources. Implementation of
442 APCDs (i.e., selective catalytic reduction, electrostatic precipitators, and wet flue gas desulfurization)
443 during coal combustion is the major factor inducing significant Hg isotope MDF during coal
444 combustion (Sun, Heimburger, et al., 2013; Tang et al., 2017). In China, the implementation level
445 of selective catalytic reductions, electrostatic precipitators, and/or wet flue gas desulfurization in
446 CFPPs is 100%, while the level in coal combustion in industrial boiler and domestic heating is
447 <12% (Wu et al., 2016). Therefore, GEM emitted from industrial boilers and domestic heating
448 in China should have much lower $\delta^{202}$Hg compared to that (0.54 ± 0.25‰, 1σ) of CFPPs
449 sufficiently equipped by APCDs (Tang et al., 2017). In addition, mean (±1σ) $\delta^{202}$Hg of Hg in
450 limestone, Hg ores, and biomass in China are —1.40 ± 0.51‰, —0.79 ± 0.14‰, and —2.97 ±
451 0.54‰, respectively, lower than those ( —0.55 ± 0.58‰, —0.59 ± 0.81‰, and —2.22 ± 0.22‰,

452 respectively) found in other regions worldwide (Demers et al., 2013; Smith et al., 2008; Sonke
453 et al., 2010; Sun et al., 2016; Thibodeau et al., 2016; Yin et al., 2013; Yu et al., 2016; Zheng et
454 al., 2016). GEM emitted from cement production preserves the Hg isotope com- position of
455 limestone and $\delta^{202}$Hg of GEM emitted from Hg production is approximately shifted by —1.12‰
456 relative to Hg ores (Sun et al., 2016). Biomass burning on average releases 95.6% of Hg to the
457 atmosphere primarily (>95%) in the form of GEM (Friedli et al., 2001) and is expected to induce
458 little Hg isotope fractionation, and therefore, the $\delta^{202}$Hg of GEM emitted should be nearly the
459 same as that in biomass. These sources account for ~62% of the total anthropogenic GEM
460 emissions in China (Zhang et al., 2015), sufficiently signifi- cant to cause a negative shift in
461 domestic GEM $\delta^{202}$Hg. Taking into account the proportions of GEM emission of the specific
462 source sectors in total anthropogenic emissions in China and their $\delta^{202}$Hg and $\Delta^{199}$Hg signa-
463 tures in Table S4 in the supporting information (Fu et al., 2017; Sun et al., 2016; Tang et al.,
464 2017; Wang et al., 2016; Yin et al., 2015, 2013, 2016; Yu et al., 2016; Zhang et al., 2015), we
465 estimate that the mean (±1σ) $\delta^{202}$Hg and $\Delta^{199}$Hg for anthropogenic GEM emissions in China are
466 —0.82 ± 0.63‰ and —0.04 ± 0.13% (Table S4), respectively. The estimated $\delta^{202}$Hg of GEM
467 emissions in China is comparatively lower than the mean value ( — 0.59‰) of global
468 anthropogenic sources predicted by Sun et al (Sun et al., 2016) but comparatively higher than that
469 (—1.79 ± 0.24‰, 1σ) estimated using the mixing diagram. The more negative $\delta^{202}$Hg signature
470 esti- mated using the mixing diagram could be partly attributed to in-plume reduction of GOM
471 emitted from anthropogenic sources. Recent studies suggested that 0–55% of emitted GOM by
472 CFPPs was reduced to GEM in plume (Landis et al., 2014). GOM emitted by anthropogenic
473 sources were estimated to have negative $\delta^{202}$Hg values of — 0.77‰ (Sun et al., 2016), and
474 reductions of GOM might further shift the isotopic composition of GEM product toward more

475 negative $\delta^{202}$Hg values (Bergquist & Blum, 2007; Zheng & Hintelmann, 2009). In addition, soil
476 GEM emission is another factor for the highly negative GEM $\delta^{202}$Hg observed in China. Soil
477 GEM emissions are much higher in China than that in the rest of the world (Wang et al., 2016;
478 Zhu et al., 2016). GEM emissions from naturally Hg-enriched soils in China have significantly
479 negative $\delta^{202}$Hg (—4.64‰ to —1.10‰, mean [±1σ] = —2.84 ± 0.67‰, *n* = 50) and positive
480 $\Delta^{199}$Hg (—0.06‰ to 0.88‰, mean [±1σ] = 0.27 ± 0.18‰, n = 50; Fu et al., 2017). Combined
481 anthropogenic and soil emissions in China yield mean (±1σ) $\delta^{202}$Hg and $\Delta^{199}$Hg of 2.04 ± 0.65‰
482 and 0.15 ± 0.15% (Table S4), respectively, which are comparable to our estimates of GEM
483 emissions in mainland China.

484 It is challenging to quantify the isotopic signatures of background atmospheric GEM pool in East
485 Asia because all the integrated GEM samples collected here were a mixture of Hg emitted from
486 the sources and back- ground atmospheric pool (Table S1). As shown in Figures 1 and S3,
487 atmospheric GEM at HNI with concentrations lower than the background (e.g., 1.5 ng/m$^3$) in the
488 Northern Hemisphere were mostly related to air masses from open seas of ECS and Yellow Sea
489 and the free troposphere over Northeast Asia, whereas GEM with concentrations higher than 1.5
490 ng/m$^3$ were mostly related to outflow of Hg from mainland China. Therefore, atmospheric GEM
491 with concentrations lower than 1.5 ng/m$^3$ reflected a minor influence of direct Hg emissions and
492 likely represented the background of atmospheric GEM in East Asia. At HNI, 16.4% of the total
493 7264 observations (5-min mean measured by Tekran system) had GEM concentrations less than
494 background of 1.50 ng/m$^3$. The average concentration of these background GEM samples
495 was1.36 ± 0.10 ng/m$^3$. This value is well within the range (—1.20–1.5 ng/m$^3$) estimated by
496 modeling studies (Pan et al., 2006; Strode et al., 2008). Hence, the $\delta^{202}$Hg and $\Delta^{199}$Hg signatures
497 of the regional background atmo- spheric GEM pool should be at 0.58‰ and 0.26‰, respectively.

498 The $\Delta^{199}$Hg signature of the background atmospheric GEM pool in East Asia is comparable to
499 the background observations in North America and Europe (mean [±1σ]= —0.21 ± 0.04‰), while
500 the $\delta^{202}$Hg signature of GEM was relatively lower than the back- ground observations in North
501 America and Europe (mean (±1σ) = 0.84 ± 0.22‰; Demers et al., 2013, 2015; Enrico et al., 2016;
502 Fu, Marusczak, Wang, et al., 2016; Obrist et al., 2017).

503

504 **CONCLUSION**

505 In this study, atmospheric GEM, PBM, and GOM concentrations and GEM isotopic composition
506 were measured at HNI in the MBL of ECS, which regularly received Hg-polluted plumes from
507 mainland China and clean air masses from open seas and free troposphere in East Asia. The data
508 set provided an evidence that outflow of Hg from mainland China strongly influenced the
509 concentrations and isotopic compositions of atmospheric GEM in the MBL of Asia marginal seas.
510 On the basis of the observations, we suggest that GEM emissions in mainland China are
511 characterized by highly negative $\delta^{202}$Hg (—1.79 ± 0.24‰, 1σ) and near-zero $\Delta^{199}$Hg (0.02 ±
512 0.04‰, 1σ) signatures, and the background regional atmospheric GEM pool was characterized
513 by moderate positive $\delta^{202}$Hg (0.58‰) and negative $\Delta^{199}$Hg (—0.26‰), providing an useful clue
514 to track the impact of Chinese Hg emissions on regional and global atmospheric GEM budget.
515 Highly negative $\delta^{202}Hg_{GEM}$ signature of Chinese Hg emissions suggested a larger contribution of
516 GEM emissions from coal combustion lacking conventional APCDs, cement and mercury
517 production, biomass burning, and soil emis- sions to the total GEM emissions in China. We
518 caution that due to the poor understanding of isotopic com- positions of GEM emitted from
519 various emission sources and fractionation processes of Hg isotopes during atmospheric

transformations, use of isotopic signatures for atmospheric Hg source apportionment still has large uncertainties. Therefore, more research regarding the isotopic compositions of Hg emitted from various anthropogenic and natural sources as well as the transformation induced fractionation of atmospheric Hg isotopes is needed.

## ACKNOWLEDGMENTS

This work was funded by the National Science Foundation of China (41622305 and 41473025), the CAS "Light of West China" program, and Youth Innovation Promotion Association, CAS (2017443). All the GEM, PBM, and GOM concentrations and GEM isotopic compositions as well as ancillary parameters used are listed in the supporting information and references.

## LIST OF FIGURES

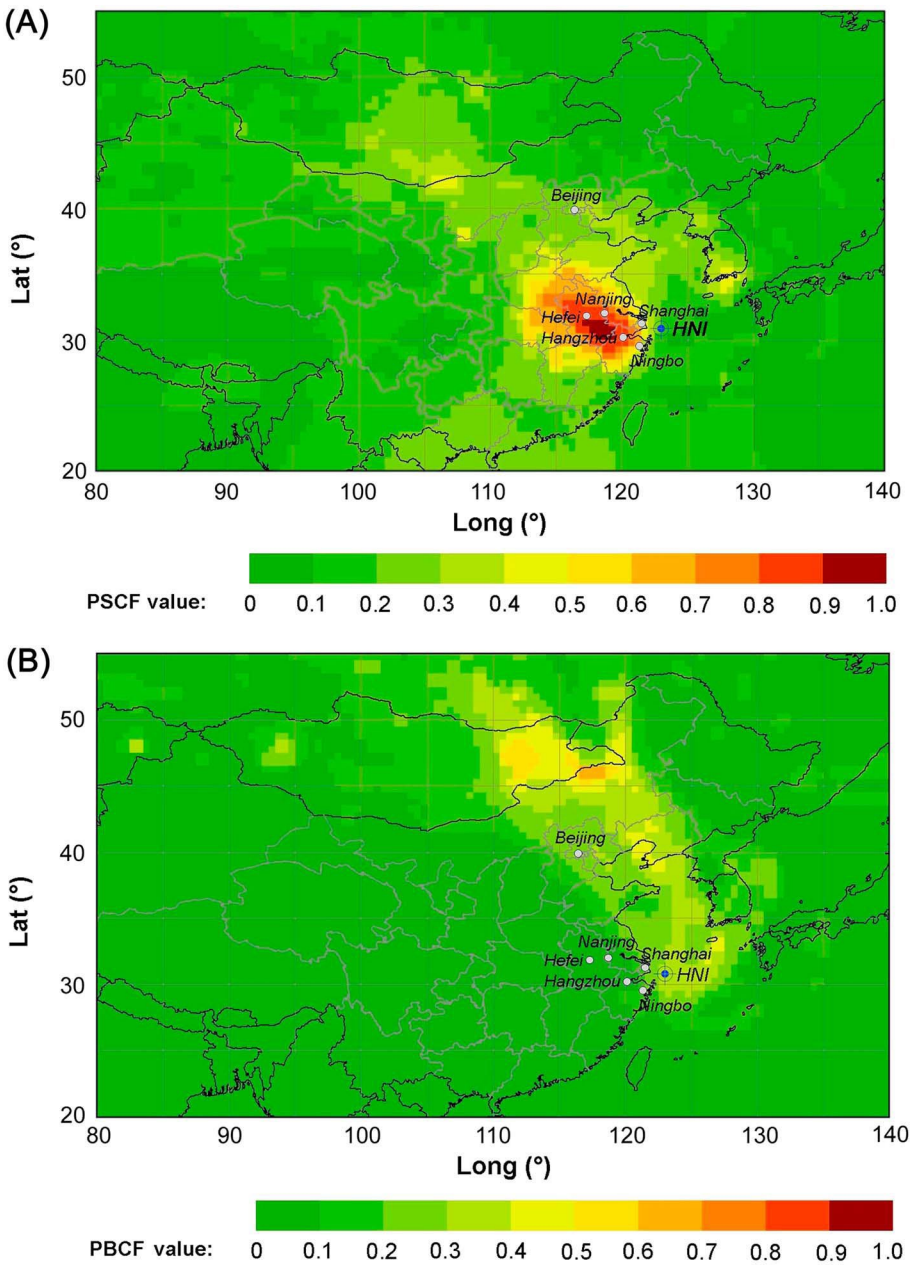


532

533 Figure 1. Potential source regions associated with (a) elevated atmospheric GEM
534 concentrations (>1.5 ng/m$^3$) and (b) low atmospheric GEM concentration (<1.5 ng/m$^3$) at
535 HNI, ECS.

536

537

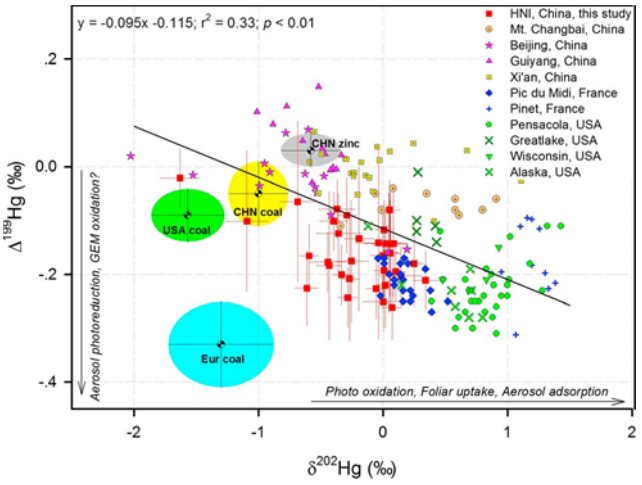


538

539 Figure 2. Mass-dependent ($\delta^{202}$Hg) and mass-independent ($\Delta^{199}$Hg) isotope signatures of
540 atmospheric TGM/GEM and source materials (e.g., China, United States, and European feed
541 coal and China zinc ores) worldwide. The error bar on $\delta^{202}$Hg and $\Delta^{199}$Hg of atmospheric GEM
542 at HNI and source materials indicates 2σ and 1σ of isotopic measurement, respectively. The
543 black line represents the relationship between GEM $\delta^{202}$Hg and $\Delta^{199}$Hg for the global
544 observations. Data are from this study and the literature (Demers et al., 2013, 2015; Enrico et al.,
545 2016; Fu, Marusczak, Wang, et al., 2016; Fu, Zhu, et al., 2016; Gratz et al., 2010; Lefticariu et
546 al., 2011; Obrist et al., 2017; Sun et al., 2014; Yin et al., 2014, 2016; Yu et al., 2016).

547

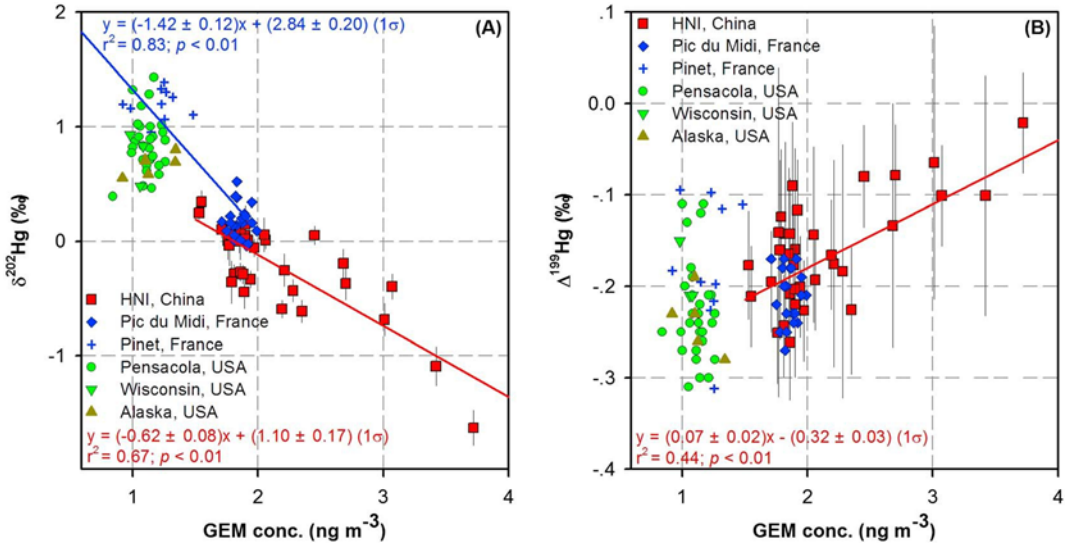


548

549 Figure 3. Relationship between atmospheric GEM concentrations and (a) GEM $\delta^{202}$Hg and
550 (b) GEM $\Delta^{199}$Hg (error bars on GEM $\delta^{202}$Hg and $\Delta^{199}$Hg indicates 2σ uncertainty) in this
551 study, Europe, North America, and Arctic. Data are from this study and the literature

(Demers et al., 2013, 2015; Enrico et al., 2016; Fu, Marusczak, Wang, et al., 2016; Obrist et al., 2017).

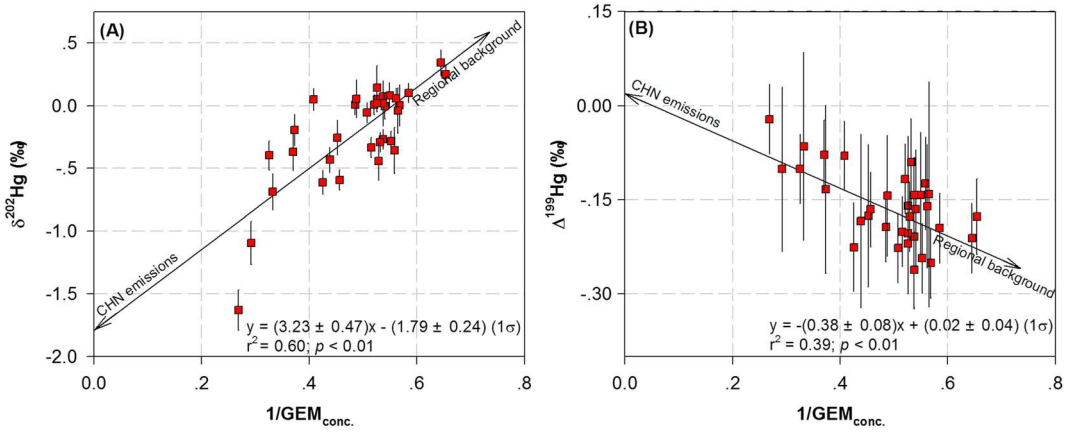


Figure 4. (a) $\delta^{202}$Hg versus 1/GEM and (b) $\Delta^{199}$Hg versus 1/GEM diagrams suggesting a binary mixing of regional back- ground atmospheric GEM pool and Chinese (CHN) emissions of GEM.

## REFERENECES


Bergquist, B. A., & Blum, J. D. (2007). Mass-dependent and -independent fractionation of Hg isotopes by photoreduction in aquatic systems. *Science*, *318*(5849), 417–420. https://doi.org/10.1126/science.1148050

Biswas, A., Blum, J. D., Bergquist, B. A., Keeler, G. J., & Xie, Z. Q. (2008). Natural mercury isotope variation in coal deposits and organic soils. *Environmental Science & Technology*, *42*(22), 8303–8309. https://doi.org/10.1021/Es801444b

Blum, J. D., & Bergquist, B. A. (2007). Reporting of variations in the natural isotopic composition of mercury. *Analytical and Bioanalytical Chemistry*, *388*(2), 353–359. https://doi.org/10.1007/s00216-007-1236-9

Blum, J. D., Sherman, L. S., & Johnson, M. W. (2014). Mercury isotopes in Earth and environmental sciences. *Annual Review of Earth and Planetary Sciences*, *42*(1), 249–269. https://doi.org/10.1146/annurev-earth-050212-124107

Chand, D., Jaffe, D., Prestbo, E., Swartzendruber, P. C., Hafner, W., Weiss-Penzias, P., et al. (2008). Reactive and particulate mercury in the Asian marine boundary layer. *Atmospheric Environment*, *42*(34), 7988–7996. https://doi.org/10.1016/j.atmosenv.2008.06.048

Chen, H. S., Wang, Z. F., Li, J., Tang, X., Ge, B. Z., Wu, X. L., et al. (2015). GNAQPMS-Hg v1.0, a global nested atmospheric mercury transport model: Model description, evaluation and

application to trans-boundary transport of Chinese anthropogenic emissions. *Geoscientific Model Development*, *8*(9), 2857–2876. https://doi.org/10.5194/gmd-8-2857-2015

Chen, J. B., Hintelmann, H., Feng, X. B., & Dimock, B. (2012). Unusual fractionation of both odd and even mercury isotopes in precipitation from Peterborough, ON, Canada. *Geochim Cosmochim Ac*, *90*, 33–46. https://doi.org/10.1016/j.gca.2012.05.005

Chen, L., Wang, H. H., Liu, J. F., Tong, Y. D., Ou, L. B., Zhang, W., et al. (2014). Intercontinental transport and deposition patterns of atmospheric mercury from anthropogenic emissions. *Atmospheric Chemistry and Physics*, *14*(18), 10,163–10,176. https://doi.org/10.5194/ acp-14-10163-2014

Cheng, I., Xu, X., & Zhang, L. (2015). Overview of receptor-based source apportionment studies for speciated atmospheric mercury.

*Atmospheric Chemistry and Physics*, *15*(14), 7877–7895. https://doi.org/10.5194/acp-15-7877-2015

Demers, J. D., Blum, J. D., & Zak, D. R. (2013). Mercury isotopes in a forested ecosystem: Implications for air-surface exchange dynamics and the global mercury cycle. *Global Biogeochemical Cycles*, *27*, 222–238. https://doi.org/10.1002/Gbc.20021

Demers, J. D., Sherman, L. S., Blum, J. D., Marsik, F. J., & Dvonch, J. T. (2015). Coupling atmospheric mercury isotope ratios and meteorology to identify sources of mercury impacting a coastal urban-industrial region near Pensacola, Florida, USA. *Global Biogeochemical Cycles*, *29*, 1689–1705. https://doi.org/10.1002/2015GB005146

Engstrom, A., & Magnusson, L. (2009). Estimating trajectory uncertainties due to flow dependent errors in the atmospheric analysis. *Atmospheric Chemistry and Physics*, *9*(22), 8857–8867. https://doi.org/10.5194/acp-9-8857-2009

Enrico, M., Le Roux, G., Marusczak, N., Heimburger, L. E., Claustres, A., Fu, X. W., et al. (2016). Atmospheric mercury transfer to peat bogs dominated by gaseous elemental mercury dry deposition. *Environmental Science & Technology*, *50*(5), 2405–2412. https://doi.org/10.1021/ acs.est.5b06058

Estrade, N., Carignan, J., Sonke, J. E., & Donard, O. F. X. (2009). Mercury isotope fractionation during liquid-vapor evaporation experiments. *Geochimica et Cosmochimica Acta*, *73*(10), 2693–2711. https://doi.org/10.1016/j.gca.2009.01.024

Estrade, N., Carignan, J., Sonke, J. E., & Donard, O. F. X. (2010). Measuring Hg isotopes in bio-geo-environmental reference materials. *Geostandards and Geoanalytical Research*, *34*(1), 79–93. https://doi.org/10.1111/j.1751-908X.2009.00040.x

Friedli, H. R., Radke, L. F., & Lu, J. Y. (2001). Mercury in smoke from biomass fires. *Geophysical Research Letters*, *28*, 3223–3226. https://doi.org/

10.1029/2000GL012704

Fu, X., Marusczak, N., Wang, X., Gheusi, F., & Sonke, J. E. (2016). Isotopic composition of gaseous elemental mercury in the free troposphere of the Pic du Midi Observatory, France. *Environmental Science & Technology*, *50*(11), 5641–5650. https://doi.org/10.1021/acs.est.6b00033

Fu, X., Zhu, W., Zhang, H., Sommar, J., Yu, B., Yang, X., et al. (2016). Depletion of atmospheric gaseous elemental mercury by plant uptake at Mt. Changbai, Northeast China. *Atmospheric Chemistry and Physics*, *16*(20), 12,861–12,873. https://doi.org/10.5194/acp-16-12861-2016

Fu, X. W., Heimburger, L. E., & Sonke, J. E. (2014). Collection of atmospheric gaseous mercury for stable isotope analysis using iodine- and chlorine-impregnated activated carbon traps. *Journal of Analytical Atomic Spectrometry*, *29*(5), 841–852. https://doi.org/10.1039/C3ja50356a

Fu, X. W., Marusczak, N., Heimburger, L. E., Sauvage, B., Gheusi, F., Prestbo, E. M., & Sonke, J. E. (2016). Atmospheric mercury speciation dynamics at the high-altitude Pic du Midi Observatory, southern France. *Atmospheric Chemistry and Physics*, *16*(9), 5623–5639. https://doi. org/10.5194/acp-16-5623-2016

Fu, X. W., Tan, Q. Y., & Feng, X. B. (2017). Mercury isotope fractionation during thermal- and photo-induced emission of Hg0 from soil. Paper presented at Proceedings of 13th International Conference on Mercury as a Global Pollutant, Providence, Rhode Island.

Fu, X. W., Zhang, H., Yu, B., Wang, X., Lin, C. J., & Feng, X. B. (2015). Observations of atmospheric mercury in China: A critical review. *Atmospheric Chemistry and Physics*, *15*(16), 9455–9476. https://doi.org/10.5194/acp-15-9455-2015

Gratz, L. E., Keeler, G. J., Blum, J. D., & Sherman, L. S. (2010). Isotopic composition and fractionation of mercury in Great Lakes precipitation and ambient air. *Environmental Science & Technology*, *44*(20), 7764–7770. https://doi.org/10.1021/Es100383w

Gustin, M. S., Amos, H. M., Huang, J., Miller, M. B., & Heidecorn, K. (2015). Measuring and modeling mercury in the atmosphere: A critical review. *Atmospheric Chemistry and Physics*, *15*(10), 5697–5713. https://doi.org/10.5194/acp-15-5697-2015

Kritee, K., Blum, J. D., & Barkay, T. (2008). Mercury stable isotope fractionation during reduction of Hg (II) by different microbial pathways. *Environmental Science & Technology*, *42*(24), 9171–9177. https://doi.org/10.1021/Es801591k

Lamborg, C. H., Hammerschmidt, C. R., Bowman, K. L., Swarr, G. J., Munson, K. M., Ohnemus, D. C., et al. (2014). A global ocean inventory of anthropogenic mercury based on water column measurements. *Nature*, *512*(7512), 65–68. https://doi.org/10.1038/Nature13563

Landis, M. S., Ryan, J. V., ter Schure, A. F. H., & Laudal, D. (2014). Behavior of mercury emissions from a commercial coal-fired power plant: The relationship between stack speciation and near-field plume measurements. *Environmental Science & Technology*, *48*(22), 13,540–13,548. https://doi.org/10.1021/es500783t

Laurier, F., & Mason, R. (2007). Mercury concentration and speciation in the coastal and open ocean boundary layer. *Journal of Geophysical Research*, *112*, D06302. https://doi.org/10.1029/2006JD007320

Laurier, F. J. G., Mason, R. P., Whalin, L., & Kato, S. (2003). Reactive gaseous mercury formation in the North Pacific Ocean's marine boundary layer: A potential role of halogen chemistry. *Journal of Geophysical Research*, *108*(D17), 4529. https://doi.org/10.1029/2003JD003625

Lefticariu, L., Blum, J. D., & Gleason, J. D. (2011). Mercury isotopic evidence for multiple mercury sources in coal from the Illinois Basin. *Environmental Science & Technology*, *45*(4), 1724–1729. https://doi.org/10.1021/Es102875n Lin, C. J., Pan, L., Streets, D. G., Shetty, S. K., Jang, C., Feng, X., et al. (2010). Estimating mercury emission outflow from East Asia using CMAQ-Hg. *Atmospheric Chemistry and Physics*, *10*(4), 1853–1864. https://doi.org/10.5194/acp-10-1853-2010

Lindberg, S., Bullock, R., Ebinghaus, R., Engstrom, D., Feng, X. B., Fitzgerald, W., et al. (2007). A synthesis of progress and uncertainties in attributing the sources of mercury in deposition. *Ambio*, *36*(1), 19–33. https://doi.org/10.1579/0044-7447(2007)36[19:ASOPAU]2.0.CO;2

Malcolm, E. G., Keeler, G. J., & Landis, M. S. (2003). The effects of the coastal environment on the atmospheric mercury cycle. *Journal of Geophysical Research*, *108*(D12), 4357. https://doi.org/10.1029/2002JD003084

Mao, H. T., Cheng, I., & Zhang, L. M. (2016). Current understanding of the driving mechanisms for spatiotemporal variations of atmospheric speciated mercury: A review. *Atmospheric Chemistry and Physics*, *16*(20), 12,897–12,924. https://doi.org/10.5194/acp-16-12897-2016

Muntean, M., Janssens-Maenhout, G., Song, S. J., Selin, N. E., Olivier, J. G. J., Guizzardi, D., et al. (2014). Trend analysis from 1970 to 2008 and model evaluation of EDGARv4 global gridded anthropogenic mercury emissions. *Science of the Total Environment*, *494*, 337–350. https://doi.org/10.1016/j.scitotenv.2014.06.014

Obrist, D., Agnan, Y., Jiskra, M., Olson, C. L., Colegrove, D. P., Hueber, J., et al. (2017). Tundra uptake of atmospheric elemental mercury drives Arctic mercury pollution. *Nature*, *547*(7662), 201–204. https://doi.org/10.1038/nature22997

Pacyna, E. G., Pacyna, J. M., Sundseth, K., Munthe, J., Kindbom, K., Wilson, S., et al. (2010). Global emission of mercury to the atmosphere from anthropogenic sources in 2005 and projections to 2020. *Atmospheric Environment*, *44*(20), 2487–2499. https://doi.org/10.1016/j.atmosenv.2009.06.009

Pan, L., Lin, C. J., Carmichael, G. R., Streets, D. G., Tang, Y. H., Woo, J. H., et al. (2010). Study of atmospheric mercury budget in East Asia using STEM-Hg modeling system. *Science of the Total Environment*, *408*(16), 3277–3291. https://doi.org/10.1016/j.scitotenv.2010.04.039

690 Pan, L., Woo, J. H., Carmichael, G. R., Tang, Y. H., Friedli, H. R., & Radke, L. F. (2006).
691 Regional distribution and emissions of mercury in East Asia: A modeling analysis of Asian
692 Pacific Regional Aerosol Characterization Experiment (ACE-Asia) observations. *Journal of*
693 *Geophysical Research*, *111*, D07109. https://doi.org/10.1029/2005JD006381

694 Pirrone, N., Cinnirella, S., Feng, X., Finkelman, R. B., Friedli, H. R., Leaner, J., et al. (2010).
695 Global mercury emissions to the atmosphere from anthropogenic and natural sources.
696 *Atmospheric Chemistry and Physics*, *10*(13), 5951–5964. https://doi.org/10.5194/acp-10-
697 5951-2010

698 Rodriguez-Gonzalez, P., Epov, V. N., Bridou, R., Tessier, E., Guyoneaud, R., Monperrus, M.,
699 & Amouroux, D. (2009). Species-specific stable isotope fractionation of mercury during Hg
700 (II) methylation by an anaerobic bacteria (Desulfobulbus propionicus) under dark conditions.
701 *Environmental Science & Technology*, *43*(24), 9183–9188. https://doi.org/10.1021/es902206j

702 Rolison, J. M., Landing, W. M., Luke, W., Cohen, M., & Salters, V. J. M. (2013). Isotopic
703 composition of species-specific atmospheric Hg in a coastal environment. *Chemical*
704 *Geology*, *336*, 37–49. https://doi.org/10.1016/j.chemgeo.2012.10.007

705 Selin, N. E., Jacob, D. J., Park, R. J., Yantosca, R. M., Strode, S., Jaegle, L., & Jaffe, D.
706 (2007). Chemical cycling and deposition of atmospheric mercury: Global constraints from
707 observations. *Journal of Geophysical Research*, *112*, D02308.
708 https://doi.org/10.1029/2006JD007450

709 Sherman, L. S., Blum, J. D., Johnson, K. P., Keeler, G. J., Barres, J. A., & Douglas, T. A.
710 (2010). Mass-independent fractionation of mercury isotopes in Arctic snow driven by
711 sunlight. *Nature Geoscience*, *3*(3), 173–177. https://doi.org/10.1038/Ngeo758

712 Slemr, F., Angot, H., Dommergue, A., Magand, O., Barret, M., Weigelt, A., et al. (2015).
713 Comparison of mercury concentrations measured at several sites in the Southern Hemisphere.
714 *Atmospheric Chemistry and Physics*, *15*(6), 3125–3133. https://doi.org/10.5194/acp-15-3125-
715 2015

716 Smith, C. N., Kesler, S. E., Blum, J. D., & Rytuba, J. J. (2008). Isotope geochemistry of mercury
717 in source rocks, mineral deposits and spring deposits of the California Coast Ranges, USA.
718 *Earth and Planetary Science Letters*, *269*(3–4), 398–406

719 Soerensen, A. L., Sunderland, E. M., Holmes, C. D., Jacob, D. J., Yantosca, R. M., Skov, H., et
720 al. (2010). An improved global model for air-sea exchange of mercury: High concentrations
721 over the North Atlantic. *Environmental Science & Technology*, *44*(22), 8574–8580. https://doi.
722 org/10.1021/Es102032g

723 Sonke, J. E., & Blum, J. D. (2013). Advances in mercury stable isotope biogeochemistry preface.
724 *Chemical Geology*, *336*, 1–4. https://doi.org/ 10.1016/j.chemgeo.2012.10.035

725 Sonke, J. E., Schafer, J., Chmeleff, J., Audry, S., Blanc, G., & Dupre, B. (2010). Sedimentary
726 mercury stable isotope records of atmospheric and riverine pollution from two major

European heavy metal refineries. *Chemical Geology*, *279*(3–4), 90–100. https://doi.org/10.1016/ j.chemgeo.2010.09.017

Sprovieri, F., Pirrone, N., Bencardino, M., D'Amore, F., Carbone, S., Cinnirella, V., et al. (2016). Atmospheric mercury concentrations observed at ground-based monitoring sites globally distributed in the framework of the GMOS network. *Atmospheric Chemistry and Physics*, *16*(18), 11,915–11,935. https://doi.org/10.5194/acp-16-11915-2016

Sprovieri, F., Pirrone, N., Gardfeldt, K., & Sommar, J. (2003). Mercury speciation in the marine boundary layer along a 6000 km cruise path around the Mediterranean Sea. *Atmospheric Environment*, *37*, S63–S71. https://doi.org/10.1016/S1352-2310(03)00237-1

Strode, S. A., Jaegle, L., Jaffe, D. A., Swartzendruber, P. C., Selin, N. E., Holmes, C., & Yantosca, R. M. (2008). Trans-Pacific transport of mercury. *Journal of Geophysical Research*, *113*, D15305. https://doi.org/10.1029/2007JD009428

Strode, S. A., Jaegle, L., Selin, N. E., Jacob, D. J., Park, R. J., Yantosca, R. M., et al. (2007). Air-sea exchange in the global mercury cycle. *Global Biogeochemical Cycles*, *21*, GB1017. https://doi.org/10.1029/2006GB002766

Sun, R. Y., Enrico, M., Heimburger, L. E., Scott, C., & Sonke, J. E. (2013). A double-stage tube furnace-acid-trapping protocol for the pre- concentration of mercury from solid samples for isotopic analysis. *Analytical and Bioanalytical Chemistry*, *405*(21), 6771–6781. https://doi.org/10.1007/s00216-013-7152-2

Sun, R. Y., Heimburger, L. E., Sonke, J. E., Liu, G. J., Amouroux, D., & Berail, S. (2013). Mercury stable isotope fractionation in six utility boilers of two large coal-fired power plants. *Chemical Geology*, *336*, 103–111. https://doi.org/10.1016/j.chemgeo.2012.10.055

Sun, R. Y., Sonke, J. E., Heimburger, L. E., Belkin, H. E., Liu, G. J., Shome, D., et al. (2014). Mercury stable isotope signatures of world coal deposits and historical coal combustion emissions. *Environmental Science & Technology*, *48*(13), 7660–7668. https://doi.org/10.1021/Es501208a

Sun, R. Y., Streets, D. G., Horowitz, H. M., Amos, H. M., Liu, G. J., Perrot, V., et al. (2016). Historical (1850–2010) mercury stable isotope inventory from anthropogenic sources to the atmosphere. *Elementa: Science of the Anthropocene*, *4*(91), https://doi.org/10.12952/journal.elementa.000091

Swartzendruber, P. C., Jaffe, D. A., Prestbo, E. M., Weiss-Penzias, P., Selin, N. E., Park, R., et al. (2006). Observations of reactive gaseous mercury in the free troposphere at the Mount Bachelor Observatory. *Journal of Geophysical Research*, *111*, D24301. https://doi.org/10.1029/ 2006JD007415

Tang, S., Feng, C., Feng, X., Zhu, J., Sun, R., Fan, H., et al. (2017). Stable isotope composition of mercury forms in flue gases from a typical coal- fired power plant, Inner Mongolia, northern China. *Journal of Hazardous Materials*, *328*, 90–97. https://doi.org/10.1016/j.jhazmat.2017.01.014

765 Thibodeau, A. M., Ritterbush, K., Yager, J. A., West, A. J., Ibarra, Y., Bottjer, D. J., et al.
766 (2016). Mercury anomalies and the timing of biotic recovery following the end-Triassic
767 mass extinction. *Nature Communications*, *7*. https://doi.org/10.1038/ncomms11147

768 Wang, F., Saiz-Lopez, A., Mahajan, A. S., Martin, J. C. G., Armstrong, D., Lemes, M., et al.
769 (2014). Enhanced production of oxidised mercury over the tropical Pacific Ocean: A key
770 missing oxidation pathway. *Atmospheric Chemistry and Physics*, *14*(3), 1323–1335.
771 https://doi.org/ 10.5194/acp-14-1323-2014

772 Wang, X., Lin, C. J., Yuan, W., Sommar, J., Zhu, W., & Feng, X. B. (2016). Emission-
773 dominated gas exchange of elemental mercury vapor over natural surfaces in China.
774 *Atmospheric Chemistry and Physics*, *16*(17), 11,125–11,143. https://doi.org/10.5194/acp-16-
775 11125-2016

776 Wang, Y. Q., Zhang, X. Y., & Draxler, R. R. (2009). TrajStat: GIS-based software that uses
777 various trajectory statistical analysis methods to identify potential sources from long-term air
778 pollution measurement data. *Environmental Modelling and Software*, *24*(8), 938–939. https://
779 doi.org/10.1016/j.envsoft.2009.01.004

780 Wiederhold, J. G., Cramer, C. J., Daniel, K., Infante, I., Bourdon, B., & Kretzschmar, R. (2009).
781 Equilibrium mercury isotope fractionation between dissolved Hg (II) species and thiol-bound
782 Hg. *Geochimica et Cosmochimica Acta*, *73*(13), A1,438–A1,438.

783 Wright, L. P., Zhang, L. M., & Marsik, F. J. (2016). Overview of mercury dry deposition,
784 litterfall, and throughfall studies. *Atmospheric Chemistry and Physics*, *16*(21), 13,399–13,416.
785 https://doi.org/10.5194/acp-16-13399-2016

786 Wu, Q. R., Wang, S. X., Li, G. L., Liang, S., Lin, C. J., Wang, Y. F., et al. (2016). Temporal
787 trend and spatial distribution of speciated atmospheric mercury emissions in China during
788 1978–2014. *Environmental Science & Technology*, *50*(24), 13,428–13,435.
789 https://doi.org/10.1021/acs. est.6b04308

790 Xu, H., Sonke, J. E., Guinot, B., Fu, X., Sun, R., Lanzanova, A., et al. (2017). Seasonal and
791 annual variations in atmospheric Hg and Pb isotopes in Xi'an, China. *Environmental Science*
792 *& Technology*, *51*(7), 3759–3766. https://doi.org/10.1021/acs.est.6b06145

793 Yin, R. S., Feng, X. B., Chen, B. W., Zhang, J. J., Wang, W. X., & Li, X. D. (2015).
794 Identifying the sources and processes of mercury in subtropical estuarine and ocean sediments
795 using Hg isotopic composition. *Environmental Science & Technology*, *49*(3), 1347–1355.
796 https://doi.org/ 10.1021/es504070y

797 Yin, R. S., Feng, X. B., & Chen, J. B. (2014). Mercury stable isotopic compositions in coals
798 from major coal producing fields in China and their geochemical and environmental
799 implications. *Environmental Science & Technology*, *48*(10), 5565–5574.
800 https://doi.org/10.1021/Es500322n

801 Yin, R. S., Feng, X. B., Foucher, D., Shi, W. F., Zhao, Z. Q., & Wang, J. (2010). High precision
802 determination of mercury isotope ratios using online mercury vapor generation system

coupled with multi-collector inductively coupled plasma-mass spectrometry. *Chinese*, *Journal of Analytical Chemistry*, *38*(7), 929–934. https://doi.org/10.3724/Sp.J.1096.2010.00929

Yin, R. S., Feng, X. B., Hurley, J. P., Krabbenhoft, D., Lepak, R. F., Hu, R. Z., et al. (2016). Mercury isotopes as proxies to identify sources and environmental impacts of mercury in sphalerites. *Scientific Reports-Uk*, (6), 18686. https://doi.org/10.1038/srep18686

Yin, R. S., Feng, X. B., Wang, J. X., Li, P., Liu, J. L., Zhang, Y., et al. (2013). Mercury speciation and mercury isotope fractionation during ore roasting process and their implication to source identification of downstream sediment in the Wanshan mercury mining area, SW China. *Chemical Geology*, *336*, 72–79. https://doi.org/10.1016/j.chemgeo.2012.04.030

Yu, B., Fu, X., Yin, R., Zhang, H., Wang, X., Lin, C.-J., et al. (2016). Isotopic composition of atmospheric mercury in China: New evidence for sources and transformation processes in air and in vegetation. *Environmental Science & Technology*, *50*(17), 9262–9269. https://doi.org/10.1021/acs.est.6b01782

Zhang, L., Wang, S. X., Wang, L., Wu, Y., Duan, L., Wu, Q. R., et al. (2015). Updated emission inventories for speciated atmospheric mercury from anthropogenic sources in China. *Environmental Science & Technology*, *49*(5), 3185–3194. https://doi.org/10.1021/Es504840m

Zhang, L. M., Wu, Z. Y., Cheng, I., Wright, L. P., Olson, M. L., Gay, D. A., et al. (2016). The estimated six-year mercury dry deposition across North America. *Environmental Science & Technology*, *50*(23), 12,864–12,873. https://doi.org/10.1021/acs.est.6b04276

Zheng, W., Foucher, D., & Hintelmann, H. (2007). Mercury isotope fractionation during volatilization of Hg(0) from solution into the gas phase. *Journal of Analytical Atomic Spectrometry*, *22*(9), 1097–1104. https://doi.org/10.1039/B705677j

Zheng, W., & Hintelmann, H. (2009). Mercury isotope fractionation during photoreduction in natural water is controlled by its Hg/DOC ratio. *Geochimica et Cosmochimica Acta*, *73*(22), 6704–6715. https://doi.org/10.1016/j.gca.2009.08.016

Zheng, W., Obrist, D., Weis, D., & Bergquist, B. A. (2016). Mercury isotope compositions across North American forests. *Global Biogeochemical Cycles*, *30*, 1475–1492. https://doi.org/10.1002/2015GB005323

Zhu, W., Lin, C. J., Wang, X., Sommar, J., Fu, X. W., & Feng, X. B. (2016). Global observations and modeling of atmosphere-surface exchange of elemental mercury: A critical review. *Atmospheric Chemistry and Physics*, *16*(7), 4451–4480. https://doi.org/10.5194/acp-16-4451-2016